Int. J. Electrochem. Sci., 15 **(2020)** 10979 – 10993, doi: 10.20964/2020.11.35

International Journal of
ELECTROCHEMICAL
SCIENCE
www.electrochemsci.org

Porous Carbon Derived from Nutshell as Electrode Materials for Supercapacitors

Yu-Long Xie[*], *Qian-Ni Guo, Cuo-Ji Ben, Li-Fang Guo*

Key Laboratory of Resource Chemistry and Eco-environmental Protection in Tibetan Plateau of State Ethnic Affairs Commission, School of Chemistry and Chemical Engineering, Qinghai Nationalities University, Xining, Qinghai, 810007, China
[*]E-mail: yulongxie2012@126.com

Received: 9 June 2020 / *Accepted:* 9 September 2020 / *Published:* 30 September 2020

The porous activated carbons derived from walnut epicarp is utilized as activated carbon electrodes for supercapacitors. The field emission scanning microscope and transmission electron microscopy tests demonstrate that the nutshell porous activated carbons (WEPACs) treated with $ZnCl_2$ can produce a large number of mesopores. As an electrode material for supercapacitor, the WEPACs possess high specific capacitance of 235 $F{\cdot}g^{-1}$ at a current density of 0.5 $A{\cdot}g^{-1}$ in three−electrode systems. As assembled WEPACs//WEPACs symmetric supercapacitor device exhibits specific energies of 17.1 $Wh{\cdot}kg^{-1}$ at a power density of 299 $W{\cdot}kg^{-1}$ and in the voltage range of 0−1.2 V. Moreover, it retaineds about 90.3% of the initial capacitance after 5000 charge−discharge cycles, indicating an excellent cyclic stability.

Keywords: Porous carbon, Supercapacitors, High energy density

1. INTRODUCTION

Supercapacitors, as promising energy storage devices, have attracted more and more attention due to the higher energy densities, faster charging rate, higher power densities, longer cycling life and better operation safety than traditional batteries. For these reasons, supercapacitor has a broad application in portable elec-tronic equipment, electrical car, and so on [1-10]. According the mechanisms, supercapacitors can be generally divided into two types, the electrical double layer capacitors (EDLCs) and pseudo-capacitors. The storing energy of EDLCs is based on electrostatic attraction to generate charge accumulation at the electrode/electrolyte interface in the electrical double-layers, while the storing energy of pseudo-capacitors is stored by the fast and reversible redox reactions at the surface of the activated electrode materials [11-14]. It is generally accepted that the performance of supercapacitors greatly depends on the electrode materials [10]. Much efforts have been and are being exerted to explore

new materials for ideal supercapacitor electrodes regarding the carbon materials [15-19], conducting polymers [20, 21], different transition metal oxides [22, 23]. Carbon materials is mainly based on the specific surface area of porous carbon electrode, such as activated carbon and mesoporous carbon, this essentially depends on the electric double layer capacitance by ion adsorbed on the surface of electrode materials. Carbon materials are widely used as electrode materials, which are also one of the most common and important candidates of supercapacitor electrode because of their outstanding cycle ability, high conductivity, large surface area, availability, and low-cost [24-27].

The incorporation of heteroatoms, especially nitrogen doped carbon materials can greatly increase the specific capacitance, because the containing nitrogen functional groups can improve the wettability of carbon materials to electrolyte solution, enhancing the electronic conductivity, while maintaining the well cycle performance [28-30]. Consequently, it is important to find an simple method and a new precursor which is high nitrogen content, cheap and environmental friendly to prepare nitrogen doped carbon materials. Recently, renewable waste biomass for preparation of activated carbon used for supercapacitor electrodes has become of great interest to use for energy storage on a large scale around the world [31-33]. In fact, many waste biomass such as lignocellulosic, wood, sunflower marrow, and orange peel are potential sources of activated carbon materials. The biomass activated carbon displays well electrochemical performance due to the moderate pore size distribution, large specific surface area and rich oxygen and nitrogen containing functional groups on the surface [34]. Therefore, it is significant to prepare biomass activated carbons, which have a high additional value and wide range of application from waste biomass.

In this paper, we present an effective synthetic route to prepare active carbons from the walnut epicarp, and the nutshell porous activated carbons (WEPACs) were activated by $ZnCl_2$ to improve their pore structures and surface performances. The influence of chemical activation on capacitances and the surface properties of the WEPACs were observed, in addition to the three electrode and two electrode cells were fabricated to estimate the electrochemical performance of the WEPACs electrode.

2. EXPERIMENTAL

2.1 Materials and Synthesis of porous activated carbon

All chemical reagents were in analytical grade.

The WEPACs was prepared from walnut epicarp, the certain amount of the nutshell sample was carbonized at 800 °C for 3 h in a tube furnace under argon protection. The prepared WEPACs were activated by $ZnCl_2$. Firstly, 1.0 g dried nutshell powder, 2.0 g $ZnCl_2$ and 50 mL pure water were mixed under stirring to form a homogeneous solution. Secondly, the homogeneous solution was transferred into a flask and kept at 105 °C under stirring to completely evaporate solvent. After that, the dried solid samples were carbonized at 850 °C for 3 h in a tube furnace under a argon atmosphere, then the products were washed with 10 wt% HCl and deionized water to remove metal ions till the filtrate became neutral. Finally, the resulting nutshell porous activated carbons were obtained after dried at 60 °C in vacuum for 12 h.

2.2 Three-Electrode Cell Fabrication

A typical three-electrode experimental cell was used to investigate the electrochemical performances of the WEPACs with a CHI 660E electrochemical workstation at room temperature. The three-electrode system equipped with a working electrode, reference electrode, and counter electrode for measuring the electrochemical properties of working electrode and its performance as a supercapacitor. The platinum foil was used as counter electrode, and a Hg/HgO as reference electrode. The working electrodes were prepared by pressing mixtures of the WEPACs, acetylene black and polytetrafluoroethylene (PTFE) binder (weight ratio of 85:10:5) onto a nickel foam current collector. All electrochemical measurements were carried out in 6 $mol \cdot L^{-1}$ aqueous KOH solution as electrolyte.

2.3 Two-Electrode Cell Fabrication

The capacitive performance of the WEPACs was further studied using a two-electrode experimental cell. The working electrodes were prepared by mixing the WEPACs with the acetylene black and PTFE binder (85:10:5) in ethanol. After that, the slurry was coated on a diameter of 1.0 cm^{-2} nickel foam and dried at 60 °C for 6 h, then used the roller to press the nickel foam into sheets under 10 MPa. The coated sample mass of each electrode was between 3.0 and 5.0 mg. When we study the sample performance, we chose two electrodes with equal or very close weight for the measurements [35]. The WEPACs electrode fitted with the separator (thin polypropylene film) and 6 $mol \cdot L^{-1}$ aqueous KOH electrolyte solution were symmetrically assembled into electrode/separator/electrode sandwich-type cells.

2.4 Characterization and electrochemical measurements

The morphologies of the WEPACs were characterized by a field emission scanning microscope (FE-SEM, Sigma 500, Carl Zeiss, Germany). X-ray diffraction (XRD) of samples was examined by a powder X-ray diffraction on Rigaku Ultima IV X-ray diffractometer with Cu Kα irradiation (λ=0.15406 nm).

The electrochemical performance of the WEPACs were studied by cyclic voltammetry (CV), galvanostic charge/discharge and electrochemical impedance spectroscopy (EIS) measurements in a typical tree-electrode system and two-electrode sandwich-type cells using a CHI 660E electrochemical workstation at room temperature. The cycle stability was investigated using cycling equipment (LAND CT2001A, Wuhan China).

3. RESULTS AND DISCUSSION

The typical FE-SEM images of the WEPACs are displays in Fig. 1, which shows the porous morphology. Fig. 1 displays abundant loose porous and three-dimensional network structure. As

prepared pristine carbon samples from nutshell have a smooth monolith surface without apparent pores (Fig. 1a).

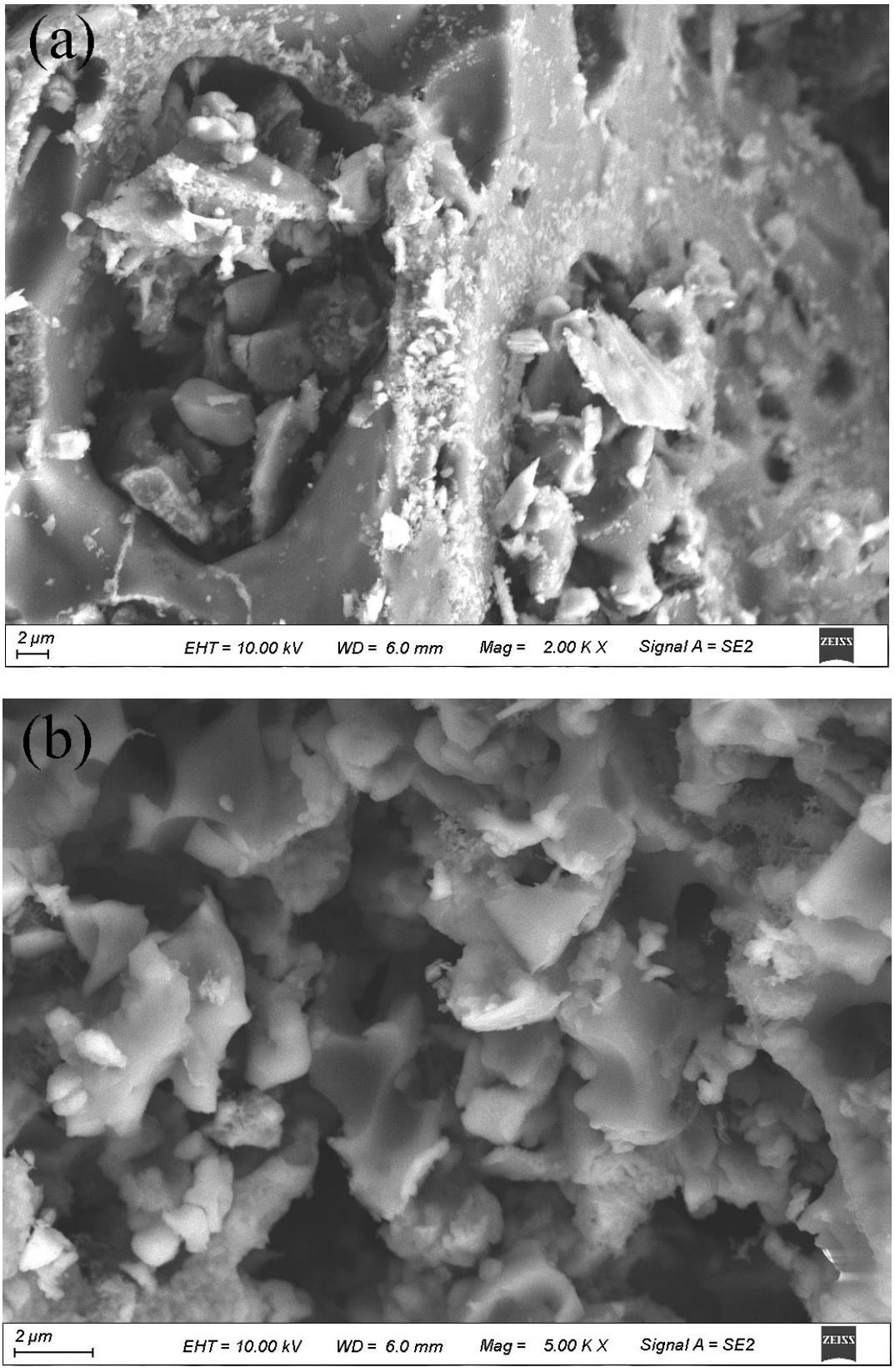

Figure 1. SEM images of WEPACs (a), and WEPACs treated with $ZnCl_2$.

However, as the sample treated with $ZnCl_2$, the surface morphology of WEPACs were changed. The WEPACs sample exhibits porous structure and rough surface (Fig. 1b), which produced high specific surface area and large pore volume.

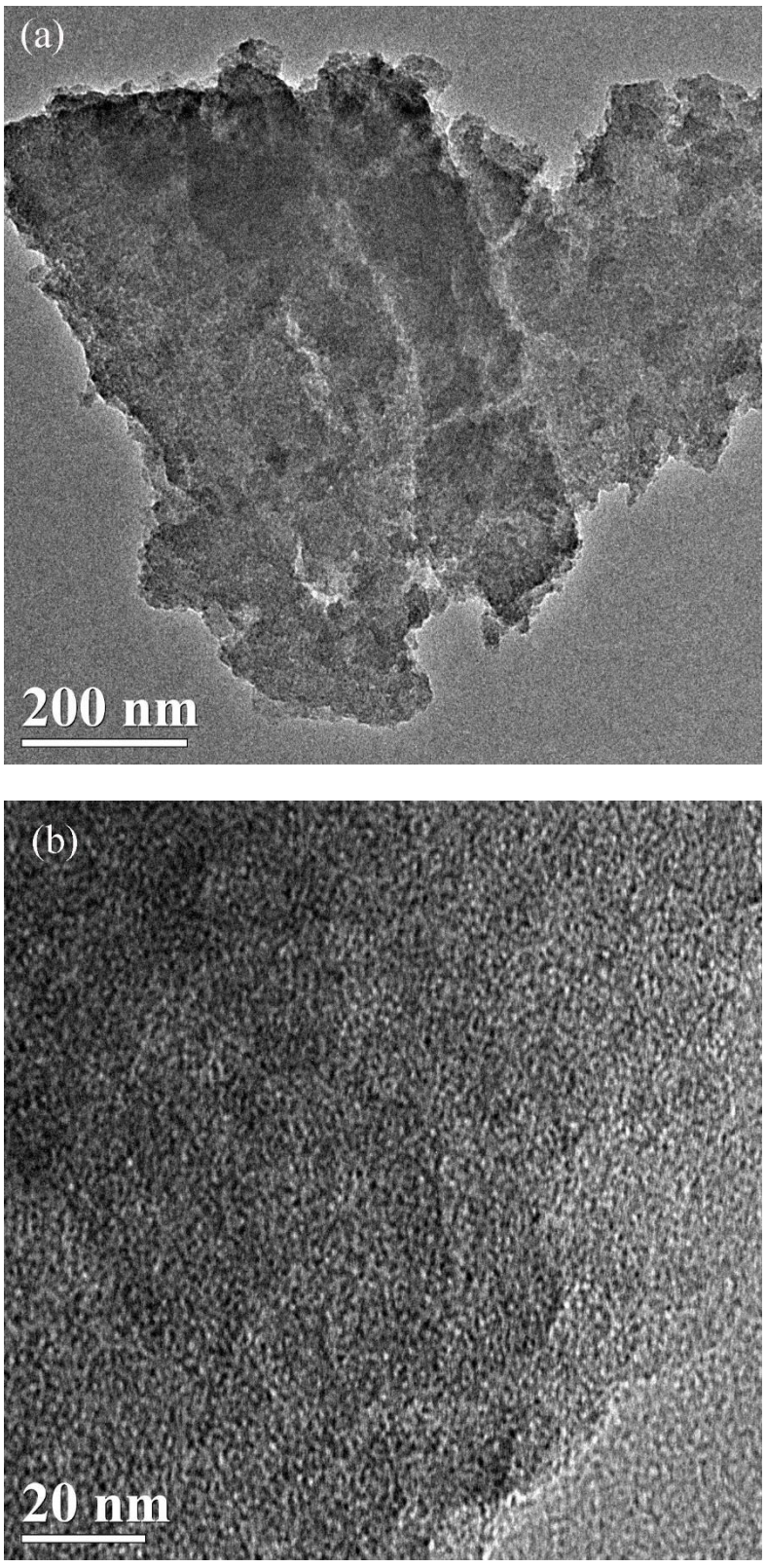

Figure 2. (a), and (b) TEM images of WEPACs under different magnification.

TEM are further employed to investigate the structure of WEPACs, the results are shown in Fig. 2a and b. As can be seen from low magnification TEM images (Fig. 2a), the WEPACs display a certain amount of pore structure, which is in agreement with the results of FE-SEM image analysis. The high-magnification TEM images are shown in Fig. 2b. The result indicate that the WEPACs may present some lattice disorder architectures and structural defects. These lattice disorder architectures and structural defects would play a significant role in electrolyte ion and charge accommodation region.

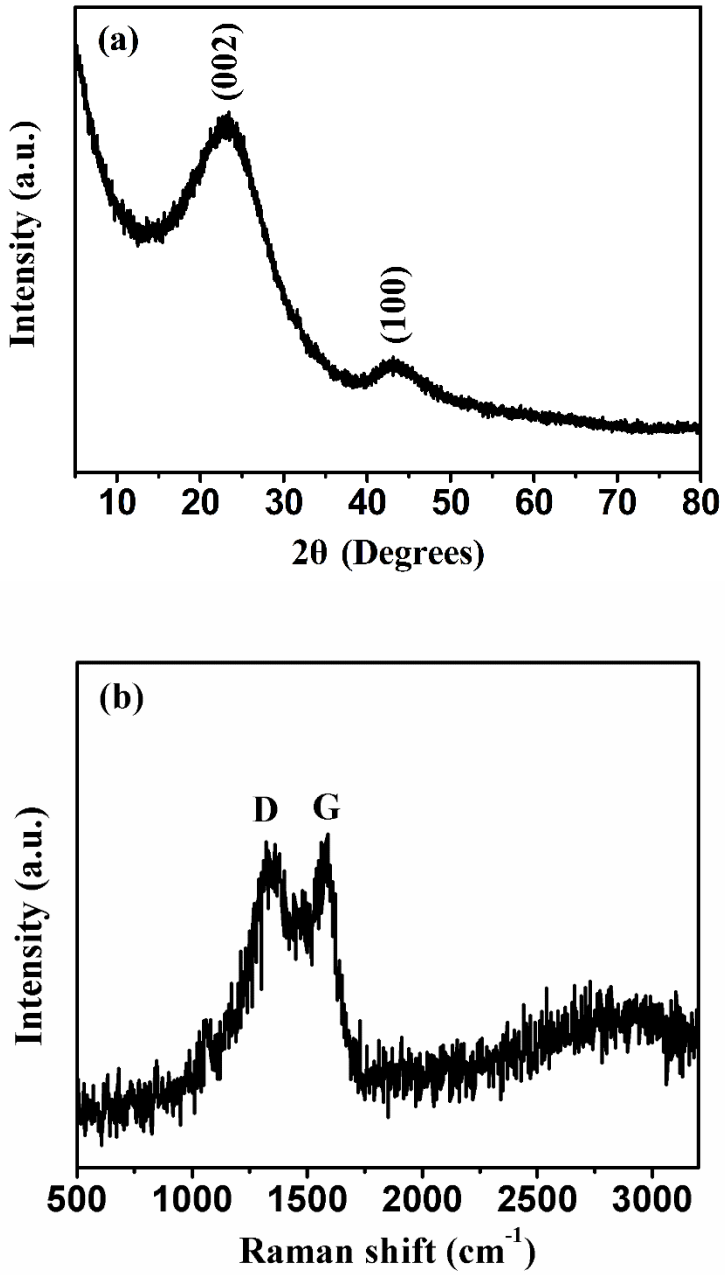

Figure 3. (a) XRD pattern and (b) Raman spectra of WEPACs.

Fig. 3a shows the XRD pattern, which exhibits two typical broad peaks at 2θ of about 23° and 43° corresponding to the (002) and (100) plane reflection. This result reveals the amorphous nature of

activated carbon. The Raman spectrum of the WEPACs is presented in Fig. 3b. As can be seen from the Raman spectra, the WEPAC shows two obvious peaks at about 1354 (D-band) and 1582 cm^{-1} (G-band), respectively.

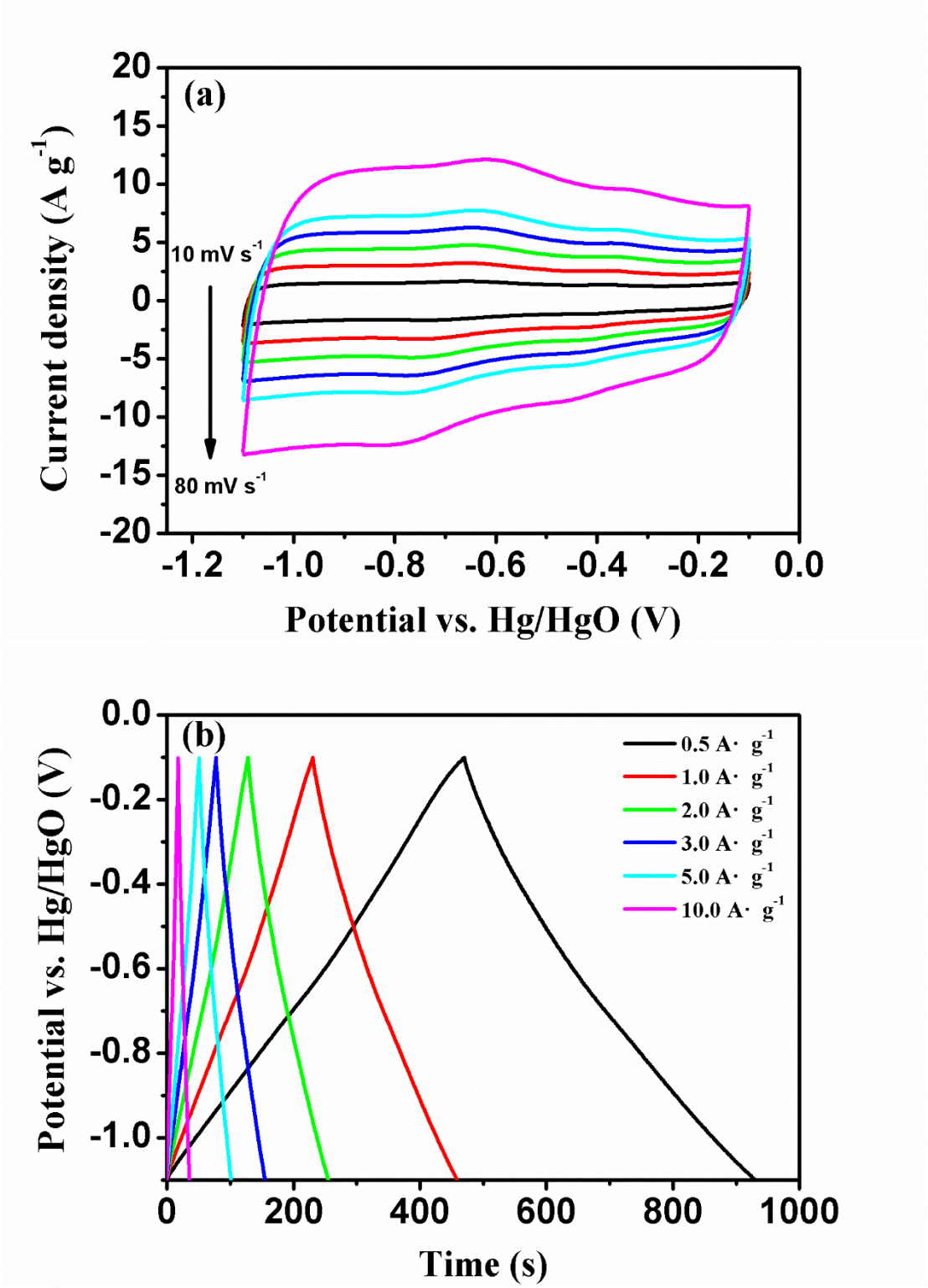

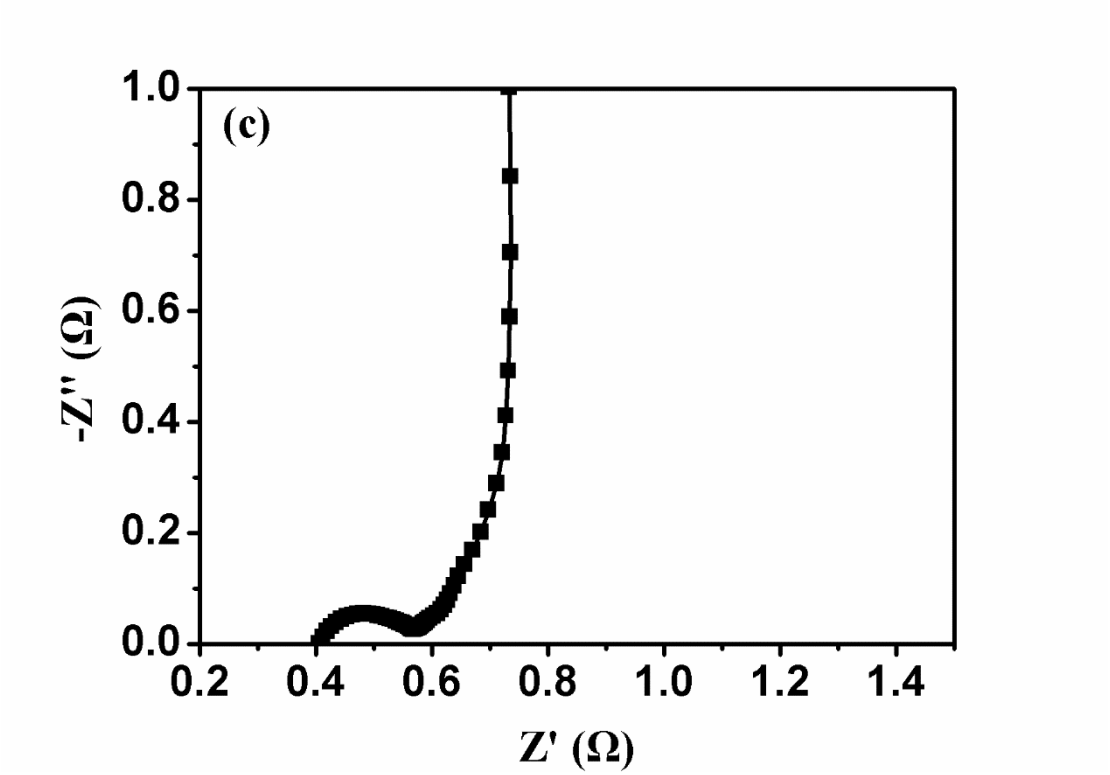

Figure 4. (a) CVs of WEPACs electrode at various scan rates from 10 to 80 $mV \cdot s^{-1}$ between −1.1 and −0.1 V (vs. Hg/HgO) in 6 M KOH aqueous solution; (b) The charge/discharge measurement of WEPACs at different current densities; (c) Nyquist plots from WEPACs electrode.

The D-band is a distinctive characteristic of the structural defects and disordered of the carbon materials, while the G-band is closely associated with a graphitic carbon phase with an sp^2 electronic configuration, such as graphene layers [36]. Furthermore, WEPACs exhibit a slightly lower intensity of D-band and a strong signal of G-band (I_D/I_G = 0.97), indicating that the WEPAC is composed of turbostratic carbon with a weakly ordered graphitic microstructure. This microstructure could play an important role in charge accommodation, and thus improve the electrical conductivity of materials.

The CVs of WEPACs electrodes were measured at a different scan rates (10−80 $mV \cdot s^{-1}$) in 6 $mol \cdot L^{-1}$ KOH electrolyte and the potential range of 0−1.2 V, respectively (Fig. 4a). The CV curves of WEPACs electrodes exhibit rectangle-like shapes. In addition, quasi-rectangular shape of the CV curves of WEPACs electrode observed even at a scan rate of up to 80 $mV \cdot s^{-1}$ (Fig. 4a), suggesting that this electrode material displays a extraordinary high rate capability. Fig. 4b shows the galvanostatic charge/discharge measurement results. The results were carried out at various current densities ranging from 0.5 to 10 $A \cdot g^{-1}$ within the potential window from −1.1 to −0.1 V of the WEPACs electrodes. The WEPACs possessed highly symmetrical galvanostatic charge/discharge curves, indicating that these electrodes have excellent electric double-layer capacitors characteristic and electrochemical reversibility. Furthermore, it is obviously that the capacitance slowly decreased with the increase of current densities. The capacitance value is 235 $F \cdot g^{-1}$ at a current density of 0.5 $A \cdot g^{-1}$, which indicates the porous and fluffy reticular structure can enhance the kinetics of ion and electron transportation at the electrode/electrolyte interface and in electrodes. Even though the current density is as high as 10 $A \cdot g^{-1}$,

the specific capacitance still maintains at a high value of about 182 $F \cdot g^{-1}$, remaining about 77% capacitance retention, suggesting an high rate capability and cycling stability. The Electrochemical impedance spectroscopy measurement for the WEPACs shown in Fig. 4c.

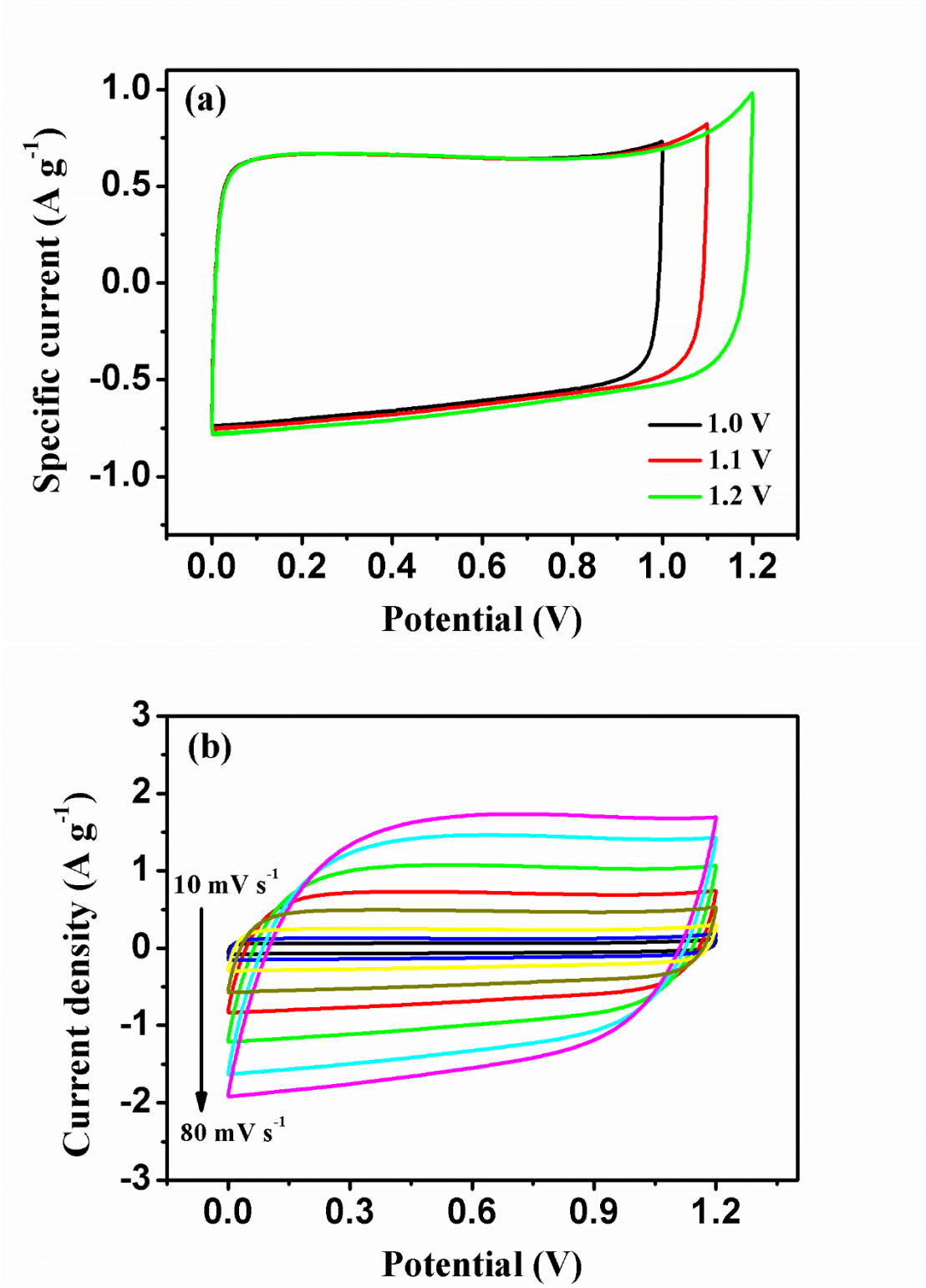

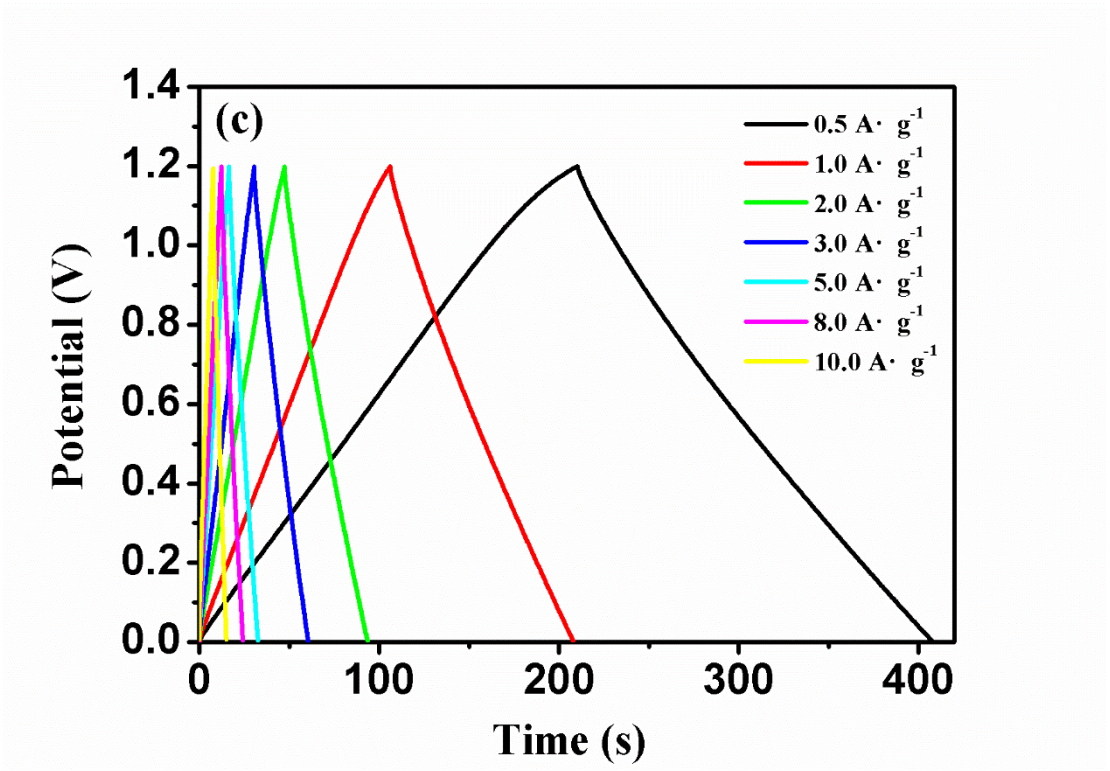
(c)
Potential (V)
Time (s)
0.5 A· g-1
1.0 A· g-1
2.0 A· g-1
3.0 A· g-1
5.0 A· g-1
8.0 A· g-1
10.0 A· g-1
0.0
0.2
0.4
0.6
0.8
1.0
1.2
1.4
0
100
200
300
400

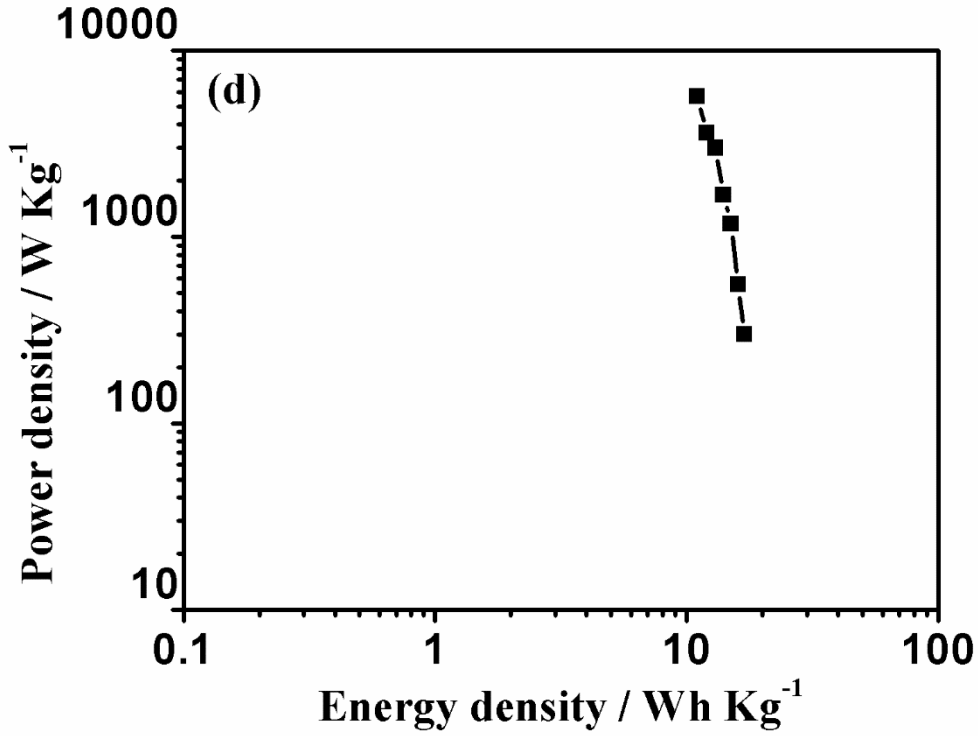
(d)
Power density / W Kg-1
Energy density / Wh Kg-1
10000
1000
100
10
0.1
1
10
100

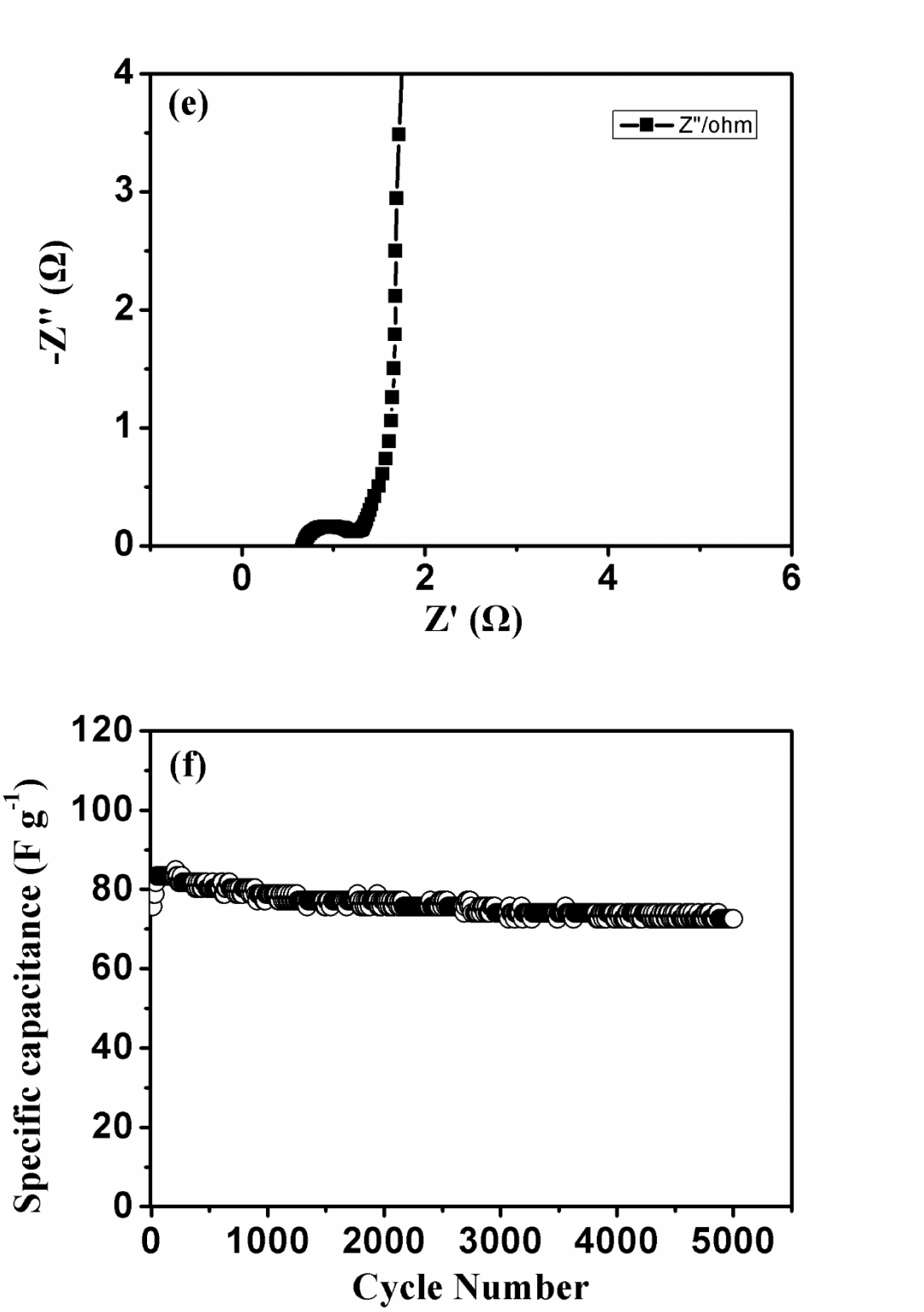

Figure 5. (a) Cyclic voltammograms of the WEPACs symmetric two electrode cell at different voltage windows in 6 M KOH electrolyte; (b) Cyclic voltammograms of the WEPACs symmetric two electrode cell at various scan rates; (c) Charge/discharge curves of WEPACs symmetric cell at various current densities; (d) Ragone plot related to energy and power densities of WEPACs symmetric cell; (e) Nyquist plots base on WEPACs symmetric two-electrode cell; (f) Cycling stability of the WEPACs symmetric two electrode cell.

It can been found, the impedance spectra of the WEPACs shows obvious semicircle at the high frequency region due to porosity of the sample and a sharp line at the low frequency region due to diffusion controlled doping and undoping of anions that result from Warburg behavior. The results indicate this materials have good electrochemical performances and electronic conductivity.

Furthermore, we also assembled symmetric two electrode supercapacitor to assess the electrochemical performance of WEPACs electrode. The as-fabricated symmetric two electrode cell was first measured at different potential windows from 1.0 to 1.2 V at 20 $mV \cdot s^{-1}$, and the results were shown in Fig. 6a. Obviously, when the high voltage increases to 1.2 V, the CV curves of the supercapacitor still remain rectangular-like shape that indicates ideal capacitive behavior and good reversibility. Therefore, the detailed investigation of WEPACs symmetric supercapacitor is performed in the voltage range of 0−1.2 V. Fig. 5b displayed the typical CV curves at different scan rates from 10 to 80 $mV \cdot s^{-1}$. We can see that the CV curve area increases with increasing scan rate, there is no obvious change and still keep a quasi-rectangular shape even at a scan rate of 80 $mV \cdot s^{-1}$. Fig. 6c shows the charge/discharge curves of the electrode at different current densities from 0.5 to 10 $A \cdot g^{-1}$, indicating a good capacitive performance of the symmetric cell. The Ragone plot of the WEPACs//WEPACs symmetric supercapacitors describing the relationship between power density and energy density in the potential range of 0−1.2 V is shown in Fig. 5d. The WEPACs//WEPACs symmetric cell displays the highest value of energy density is 17.1 $Wh \cdot kg^{-1}$ at a power density of 299 $W \cdot kg^{-1}$. At the same time, value of energy density is even remained 11.3 $Wh \cdot kg^{-1}$ at a power density of 5657 $W \cdot kg^{-1}$. These results suggest that the WEPACs materials may be a promising electrode materials for supercapacitors. The resistive and capacitive behavior was studied by using electrochemical impedance spectroscopy and exhibited in Fig. 5e. In the high-frequency region of the electrochemical impedance spectroscopy, the imaginary part (Z') of the impedance is very small and the real part of resistance (Z'') is in corresponding with the ohmic resistance from the electrolyte and the interface between the current collector and the active material (Rs). At the same time, in the low-frequency region almost vertical curve represents the ideal capacitance behavior of the carbon materials [37]. As shown in Figure 5e, the internal resistance of the test symmetric cell is 0.79 Ω, indicating the high electrical conductivity. The cycling stability of WEPACs//WEPACs symmetric cell was carried out by continuous charge/discharge cycling at a current density 1 $A \cdot g^{-1}$ for 5000 cycles, and the results were shown in Fig. 5f. The cell exhibits good cycle stability, after 5000 charge/discharge cycles, about 90.3% of the initial capacitance is retained for the WEPACs//WEPACs symmetric cell.

Table 1. Representation of the performance of porous carbon materials from various biomass carbon materials as electrodes for supercapacitors.

Biomass	Electrolyte	Specific capacitance	Current density	Ref.
Pomelo peel	1 M TEA BF4-PC	163 $F \cdot g^{-1}$	0.5 $A \cdot g^{-1}$	[37]
Bamboo	1 M H_2SO_4	318 $F \cdot g^{-1}$	0.2 $A \cdot g^{-1}$	[38]
Bamboo	6 M KOH	222.0 $F \cdot g^{-1}$	0.5 $A \cdot g^{-1}$	[39]

Rape pollen	1.0 M Na_2SO_4	361.6 $F \cdot g^{-1}$	1 $A \cdot g^{-1}$	[40]
Coconut shell	1 M $TEMABF_4$	91.15 $F \cdot g^{-1}$	0.2 $A \cdot g^{-1}$	[41]
Green tea waste	1.0 M Na_2SO_4	162 $F \cdot g^{-1}$	0.5 $A \cdot g^{-1}$	[42]
Oil-tea seed shell	6 M KOH	350.2 $F \cdot g^{-1}$	0.5 $A \cdot g^{-1}$	[43]
Walnut epicarp	6 M KOH	235 $F \cdot g^{-1}$	0.5 $A \cdot g^{-1}$	This work

Although the performance of the WEPACs for supercapacitors were not the best compared with some work reported previously (Table 1), the current density up to 10 $A \cdot g^{-1}$, the specific capacitance still maintained in a high specific capacitance value about 182 $F \cdot g^{-1}$, remaining about 77% capacitance retention, indicating an excellent rate capability and cycling stability.

4. CONCLUSIONS

In summary, we have prepared porous activated carbons using walnut epicarp by $ZnCl_2$ as activation agent, the resulting porous carbon demonstrates porous morphology, a loose, which produce large pore volume and high specific surface area. As an electrode materials for supercapacitors, the WEPACs electrode possess a maximum capacitance of 235 $F \cdot g^{-1}$ at a current density of 0.5 $A \cdot g^{-1}$ in three-electrode systems. Furthermore, the assembled WEPACs//WEPACs symmetric supercapacitor device exhibits specific energies of 17.1 $Wh \cdot kg^{-1}$ at a power density of 299 $W \cdot kg^{-1}$ and in the voltage range of 0−1.2 V. Moreover, it retaineds about 90.3% of the initial capacitance after 5000 charge−discharge cycles, indicating an excellent cyclic stability. This outstanding capacitive properties demonstrate that this porous activated carbons have great potential in developing supercapacitor with a high power density, energy density, coulombic effificiency and long-term cycle stability.

ACKNOWLEDGEMENTS
Financial support from the Research Program of Application Foundation of Qinghai Province (No. 2019-ZJ-7013).

References

1. H. Wang, H. Yi, X. Chen, X. Wang, *J. Mater. Chem*., 2 (2014) 1165–1173.
2. A.S. Aricò, P. Bruce, B. Scrosati, J.M. Tarascon, W.V. Schalkwijk, *Nat. Mater*., 4 (2005) 366–377.
3. B.Dyatkin, V. Presser, M. Heon, M.R. Lukatskaya, M. Beidaghi, Y. Gogotsi, *ChemSusChem*, 6 (2013) 2269–2280.
4. S. Han, D. Wu, S. Li, F. Zhang, X. Feng, *Adv. Mater*., 26 (2014) 849–864.
5. P. Simon, Y. Gogotsi, *Nat. Mater*., 7 (2008) 845–854.
6. R.R. Salunkhe, C. Young, J. Tang, T. Takei, Y. Ide, N. Kobayashi, Y. Yamauchi, *Chem. Commun.*, 52 (2016) 4764–4767.
7. J. Tang, Y. Yamauchi, *Nat. Chem*., 8 (2016) 638–639.

8. C. Young, R.R. Salunkhe, J. Tang, C.C. Hu, M. Shahabuddin, E. Yanmaz, M.S.A. Hossain, Y. Yamauchi, J.H. Kim, *Phys. Chem. Chem. Phys*., 18 (2016) 29308–29315.
9. N.L. Torad, R.R. Salunkhe, Y. Li, H. Hamoudi, M. Imura, Y. Sakka, Y. Yamauchi, *Chem. Euro. J*., 20 (2014) 7895–7900.
10. G. Wang, L. Zhang, J. Zhang, *Chem. Soc. Rev*., 41 (2012) 797–828.
11. G. Ren, G. Ma, N. Cong, *Renew. Sus. Energ. Rev*., 41 (2015) 225–236.
12. G. Wang, J. Zhang, S. Kuang, J. Zhou, W. Xing, S. Zhuo, *Electrochim. Acta*, 153 (2015) 273–279.
13. X. Yang, J. Zhu, L. Qiu, D. Li, *Adv. mater*., 23 (2011) 2833–2838.
14. K. Sun, Q. Yang, Y. Zheng, G. Zhao, Y. Zhu, X. Zheng, G. Ma, *Int. J. Electrochem. Sci*., 12 (2017) 2606 – 2617.
15. J. Lee, J. Ko, J. Kim, *Electrochim. Acta*, 85 (2012) 459–466.
16. R.K. Paul, M. Ghazinejad, M. Penchev, J. Lin, M. Ozkan, C.S. Ozkan, *Small*, 6 (2010) 2309–2313.
17. E.Redondo, J. Carretero-González, E. Goikolea, J. Ségalini, R. Mysyk, *Electrochim. Acta*, 160 (2015) 178–184.
18. M. Chen, X. Kang, T. Wumaier, J. Dou, B. Gao, Y. Han, L. Zhang, *J. Solid State Electr*., 17 (2013) 1005–1012.
19. K. Sun, E. Feng, H. Peng, G. Ma, Y. Wu, H. Wang, Z. Lei, *Electrochim. Acta*, 158 (2015) 361–367.
20. H.R. Ghenaatian, M.F. Mousavi, M.S. Rahmanifar, *Electrochim. Acta*, 78 (2012) 212–222.
21. L. Nyholm, G. Nyström, A. Mihranyan, M. Strømme, *Adv. Mater*., 23 (2011) 3751–3769.
22. H. Jiang, T. Zhao, C. Li, J. Ma, *J. Mater. Chem*., 21 (2011) 3818–3823.
23. S. Park, S. Kim, *Electrochim. Acta*, 89 (2013) 516–522.
24. S. SenthilKumar, R. Selvan, Y. Lee, J. Melo, *J. Mater. Chem.* A, 1 (2013) 1086–1095.
25. J. Jiang, Y.Y. Li, J.P. Liu, X.T. Huang, C.Z. Yuan, X.W.D. Lou, *Adv. Mater*., 24 (2012) 5166–5180.
26. K.J. Sun, H.P. Wang, H. Peng, Y.J. Wu, G.F. Ma, Z.Q. Lei, *Int. J. Electrochem. Sci.,* 10 (2015) 2000–2013.
27. H.C. Chen, F.G. Sun, J.T. Wang, W.C. Li, W.M. Qiao, L.C. Ling, D.H. Long, *J. Phys. Chem*. C., 117 (2013) 8318–8328.
28. Y. Zhai, Y. Dou, D. Zhao, P. F. Fulvio, R.T. Mayes., S. Dai, *Adv. Mater*., 23 (2011) 4828–4850.
29. J. Tang, J. Liu, C. Li, Y. Li, M. O. Tade, S. Dai., Y. Yamauchi, *Angew. Chem., Int. Ed*., 54 (2015) 588–593.
30. G. Ma, Z. Zhang, K. Sun, H. Peng, Q. Yang, F. Ran, Z. Lei, *RSC Adv*., 5 (2015) 107707–107715.
31. T. E. Rufford, D. Hulicova-Jurcakova, E. Fiset, Z. H. Zhu, G.Q. Lu, *Electrochem. Commun*., 11 (2009) 974–977.
32. L. Wei, G. Yushin, *Nano Energy*, 1 (2012) 552–565.
33. G.G. Choi, S.J. Oh, S.J. Lee, J.S. Kim, *Bioresource Technol*., 178 (2015) 99–107.
34. K. Wang, N. Zhao, S. Lei, R. Yan, X. Tian, J. Wang, L. Liu, *Electrochim. Acta*, 166 (2015) 1–11.
35. H. Peng, G.F. Ma, K.J. Sun, J.J. Mu, Z. Zhang, Z.Q. Lei, *ACS Appl. Mater. Inter*., 6 (2014) 20795–20803.
36. M.S. Dresselhaus, A. Jorio, M. Hofmann, G. Dresselhaus, R. Saito, *Nano Lett*., 10 (2013) 751–758.
37. F. Sun, L. Wang, Y. Peng, J. Gao, X. Pi, Z. Qu, G. Zhao, Y. Qin, *Appl. Surf. Sci.*, 436 (2018) 486–494.
38. B. Chang, Y. Guo, Y. Li, H. Yin, S. Zhang, B. Yang, X. Dong, *J. Mater. Chem. A*, 3 (2015) 9565–9577.
39. Y. Gong, D. Li, C. Luo, Q. Fu, C. Pan, *Green Chem.*, 19 (2017) 4132–4140.
40. L. Wan, W. Wei, M. Xie, Y. Zhang, X. Li, R. Xiao, J. Chen, C. Du, *Electrochim. Acta*, 311 (2019) 72–82.
41. J. Xia, N. Zhang, S. Chong, D. Li, Y. Chen, C. Sun, *Green Chem.*, 20 (2018) 694–700.
42. S. Sankar, A.T.A. Ahmed, A.I. Inamdar, H. Im, Y.B. Im, Y. Lee, D.Y. Kim, S. Lee, *Mater. Des.*, 169 (2019) 107688.

43. Y. Zhang, L. Liu, P. Zhang, J. Wang, M. Xu, Q. Deng, Z. Zeng, S. Deng, *Chem. Eng. J.*, 355 (2019) 309–319.
44. J. Yan, T. Wei, B. Shao, F. Ma, Z. Fan, M. Zhang, C. Zheng, Y. Shang, W. Qian, F. Wei, *Carbon*, 48 (2010) 1731–1737.